Theor. Appl. Climatol. 73, 207–221 (2002)
DOI 10.1007/s00704-002-0673-9

Theoretical and Applied Climatology
Printed in Austria

[1] Key Laboratory for Mesoscale Severe Weather of Ministry of Education, Nanjing University, Nanjing, China
[2] Department of Earth Science, Nanjing University, Nanjing, China
[3] Cold and Arid Regions Environmental and Engineering Research Institute, Lanzhou, China

Effects of subgrid heterogeneities in soil infiltration capacity and precipitation on regional climate: a sensitivity study

X.-M. Zeng[1,2], **M. Zhao**[1], **B.-K. Su**[1], **J.-P. Tang**[1], **Y.-Q. Zheng**[1], **Y.-J. Zhang**[3], and **J. Chen**[2]

With 9 Figures

Received June 18, 2001; revised February 14, 2002; accepted March 3, 2002
Published online October 7, 2002

Summary

One of the most pronounced features of the land surface is its heterogeneity. In order to further understand land-atmosphere interactions and improve climate modeling it is very important to investigate effects of subgrid scale heterogeneities, especially hydrological-process heterogeneities. In this paper, after the construction and sensitivity tests of a hydrological model (VXM), which accounts for precipitation heterogeneity (PH) and infiltration heterogeneity (IH), we incorporated VXM into the NCAR (National Center for Atmospheric Research) regional climate model RegCM2 and thus obtained the augmented regional climate model (hereafter, ARCM). By using 3-month (May–July) observational data of 1991 Meiyu season, we conducted numerical experiments with ARCM, analyzed the sensitivities, and found that: (1) The regional climate and surface hydrology are very sensitive to IH as well as PH, i.e., the simulations for the surface fluxes, soil temperature, soil moisture, precipitation and surface runoff can be greatly affected by those heterogeneities. (2) ARCM can effectively improve the simulation of hydrological processes, i.e., it can greatly enhance the surface runoff ratio (i.e., the ratio of surface runoff to precipitation), which is consistent with observations over humid areas in China. (3) It seems that the IH influence on the surface climate is larger than the PH influence. (4) The modeled climate is sensitive to the VXM parameters. For example, it is significantly modified after the surface impermeable fraction has been accounted for, suggesting some features of aridification.

1. Introduction

The hydrological cycle is a major component of the climate system and is characterized by pronounced land surface heterogeneities in many aspects, such as soil properties, rainfall, topography and water table elevation. In previous studies (Beven and Kirkby, 1979; Smith and Hebbert 1983; Sivapalan et al., 1987; Sivapalan et al., 1997; Yu, 2000), hydrological models have been developed to account for these heterogeneities. In the past two decades, there has been an increasing number of land surface parameterizations recognizing the importance of incorporating heterogeneities in hydrological processes (Avissar and Pielke, 1989; Koster and Suarez 1992; Famiglietti and Wood, 1994; Sellers et al., 1996; Peters-Lidard et al., 1997; Walko et al., 2000). As reviewed in Giorgi and Avissar (1997), the effects of surface heterogeneity can be grouped into the categories ‘‘aggregation’’ and ‘‘dynamical’’ effects: subgrid scale aggregation has been shown to especially affect the simulated surface latent and sensible heat fluxes, snowpack, and dynamics of soil moisture and runoff. Dynamical heterogeneity effects are associated with

microscale and mesoscale circulations induced by heterogeneous surfaces. For example, Sivapalan et al. (1997) presented a hydrological model and found that sub-grid rainfall variability, especially the partial coverage that characterizes rainfall events at such large scales, causes significant biases in the estimation of land surface fluxes; Walko et al. (2000) showed that their model accounting for heterogeneity in hydrological processes had significant effects not only in producing subgrid heterogeneity of soil moisture but also on the grid-cell-averaged surface fluxes of sensible and latent heat.

Among the subgrid heterogeneities affecting hydrological processes, we only account for two primary heterogeneities, in this paper namely, precipitation heterogeneity (PH) and infiltration heterogeneity (IH) in a grid cell of numerical models, by continuous approach (Giorgi and Avissar, 1997).

The extension of the area affected depends on the kind of precipitation, e.g., precipitation induced by large-scale air-mass lifting covers a large-scale area, while the area of precipitation induced by mere cumulus convection is much smaller. Thus, for a grid cell in a global climate model (GCM) or a regional climate model (RCM), the coverage of different kinds of precipitation is different, i.e., a smaller coverage corresponds to a smaller scale of precipitation over a smaller fraction of a grid cell, and vice visa. Besides, there is a heterogeneity in precipitation intensity in the precipitating area. All these heterogeneities can greatly affect simulations for surface climatology and hydrology, e.g., precipitation amounts in numerical models are often underestimated, and so are surface runoff. As for GCMs, the conventional spatial averaging inherent in area discretization thus restricts the generation of surface runoff to those rare cases of intensive precipitation over grid areas of low average permeability and high average water table (Entekhabi and Eagleson 1989), which is unrealistic for common land surface. It is analogous for the RCM case.

Eagleson (1984) and Eagleson et al. (1985, 1987) demonstrated that generally about 60% of storm areas are actually wetted by rainfall. Depending on the ratio of the GCM grid area to typical storm areas, this value is proportionally scaled, and it is assumed that large-scale condensation occurs over the entire storm area but convective precipitation covers 60% of total storm area (Eagleson et al., 1989). As for PH over a fraction of a grid cell, Warrilow et al. (1986) assumed the precipitation intensity is exponentially distributed, as seems appropriate in some cases, while Gao and Sorooshian (1994) found that for some conditions, the lognormal relationship might be more appropriate.

Many formulations of the infiltration capacity, have been presented, e.g., the formulas of Horton (1933) and Philip (1957), who defined their infiltration capacity as the maximum rate at which infiltration can occur, are widely used. However, most of these formulas do not account for IH. In fact, formulas without inclusion of IH may only be suitable for very uniform soil, and can no longer be applied due to the variations in topography, soil texture, etc. For example, the saturated conductivity for loam has the value of 6.3×10^{-3} mm/s (Dickinson et al., 1993), which implies that it is very hard to generate surface runoff at the loam surface even if precipitation amount/intensity is very large. However, in reality, loam is often spread at a scale of about several tens of kilometers, and surface runoff can still occur frequently. Considering the heterogeneity of infiltration storage capacity, which is defined as the water amount that can infiltrate due to more storage capacity, the Xinanjiang Model in China (Zhao, 1984) has been used operationally for flood forecasting in China and elsewhere (Francini and Pacciani, 1991). Based on the Xinanjiang model, Wood et al. (1992) developed the Variable Infiltration Capacity (VIC) Model. They found that the Geophysical Fluid Dynamics Laboratory (GFDL) bucket model runoff generally had a lot less variability than the historic streamflows for short time scales (e.g., 1 day), while the VIC model was much more similar to the observed flows in this respect. Stamm and Wood (1994) investigated the sensitivity of global climate to the characterization of the land-surface hydrology by using the GFDL GCM with the bucket model and the VIC model. Liang et al. (1994) generalized the VIC model that is comprised of a two-layer characterization of the soil coloumn and uses an aerodynamic representation of surface latent and sensible heat fluxes. They then extended the two-layer VIC model to incorporate a representation of subgrid

variability in precipitation (i.e., PH) (Liang et al., 1996).

The objective of this study is to investigate the effects of PH and IH and to further improve regional climate modeling with an RegCM2 (Giorgi et al., 1993a,b), the National Center for Atmospheric Research regional climate model, rather than a GCM. RegCM2 employs the Biosphere/Atmosphere Transfer Scheme (BATS, Dickinson et al., 1993), in which heterogeneities affecting hydrological processes are not included.

Therefore, in Section 2 of this paper, we address the construction and sensitivity tests of an off-line hydrological model that considers PH and IH; in Section 3, we modify the model and incorporate it into RegCM2, and then analyze the sensitivities of the experiments; and Section 4 presents the summary and discussions.

2. Construction and tests of the hydrological model VXM

2.1 Brief description of VXM

In order to investigate regional climate and its variation, it is very important to develop a hydrological model representing regional-scale characteristics and which is suitable for coupling with RCMs. As a first step, a regional hydrological model (for simplicity, here after referred to as VXM) is constructed here. VXM is a combination of the Xinanjiang model and the VIC model, but it is different from both, e.g., VXM takes into account the impermeable fraction that is important for semi-humid region though unimportant for humid region, while the VIC model doesn't. VXM includes the treatments for homogeneous and heterogeneous precipitations.

As for treatments for homogeneous-precipitation case (HMC), VXM also considers IH, evapotranspiration heterogeneity and therefore the effects of the heterogeneities on runoff, which is similar to the Xinanjiang model and the VIC model. Over a given area (e.g., a grid area), the heterogeneities are the results of many factors such as vegetation, soil texture and topography. Thus, IH can be represented (Fig. 1; also Eq. (A1) in appendix). Then, if the maximum soil water storage W_c and initial infiltration capacity i_0 (or initial water storage W_0) are given and, within a time step, the area receives a precipitation amount

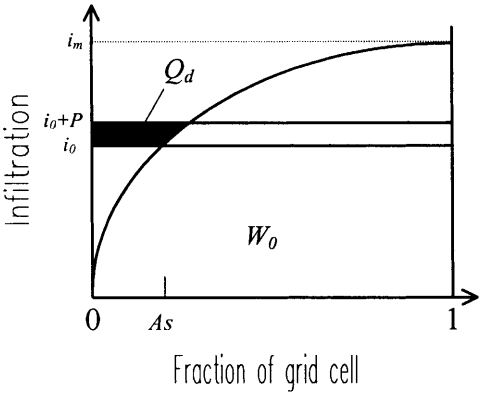

Fig. 1. Schematic of runoff-infiltration relationships for VXM (the permeable-area case)

P, the surface runoff Q_d can also be computed. In addition, Evapotranspiration and base flow are parameterized. For details, see Appendix.

Considering f_i, the impermeable fraction over the area, the above parameterization should be modified. Here we only consider precipitation and evapotranspiration for f_i, in which the precipitation amount is $P \times (1-f_i)$, and evapotranspiration e_i is empirically calculated by

$$e_i = \min[\max(4 \times 10^{-4} f_i,\ 0.08 f_i P),\ f_i E_p], \qquad (1)$$

where e_i is in units of mm, E_p the potential evapotranspiration. Thus, given B_e, the shape parameter of evapotranspiration, the total evapotranspiration can be computed by

$$E = e_i + E_p \left[1 - \left(1 - \frac{W_0}{W_c}\right)^{1/B_e}\right](1-f_i). \qquad (2)$$

Different from Zhao (1984), we do not modify the equation for W_c here, for we assume that the infiltration-runoff relation (Fig. 1) is still satisfied within the permeable fraction $(1-f_i)$, i.e., the consideration of the infiltration heterogeneity with impermeable fraction is the same as that without impermeable fraction. Therefore when $f_i > 0$, the calculations for other quantities are the same as those when $f_i = 0$, except that the quantities such as i_0 and W_c are considered within the permeable fraction.

So, the model characteristic parameters are B (water storage parameter, see appendix), W_c, B_e, k_b (base flow parameter) and f_i, and the parameters, i_0, E_p and P, are related to the time step. Given these parameters, we can compute quantities of interest, e.g., the surface runoff Q_d, water storage W_0, following Wood et al. (1992).

Besides, the treatments for heterogeneous-precipitation case (HTC) are similar to that for HMC (see Appendix 2).

2.2 Sensitivity tests of VXM parameters

2.2.1 Experimental design

We firstly design some experiments to test the sensitivity of VXM to different parameters, i.e., the model characteristic parameters B, W_c, B_e, k_b and f_i, and the parameters, i_0, E_p and P, which are associated with the time step. In the experiments, the time step is 200s, and the two input constants E_p and P are respectively transformed into E_{ps} and P_s to represent instantaneous values (mm/s).

Generally, recommended values in the literature (e.g., Stamm and Wood, 1994; Zhao, 1984) are taken here, e.g., $B = 0.3$, $W_c = 130$ mm, $B_e = 0.5$, $f_i = 0$. At the first place, we use the case when $P = 0$. With $E_{ps} = 6 \times 10^{-5}$ mm/s, $k_b = 5 \times 10^{-5}$, if initially $W_0 = 90$ mm, the evapotranspiration simulated with VXM changes from 7.1 mm to 5.2 mm in the subsequent 10 days; similarly, if initially $W_0 = 50$ mm, then the evapotranspiration changes from 4.3 mm to 2.9 mm in the subsequent 10 days. All these values are consistent with observations for the humid region of the southern part of China, e.g., the daily evapotranspiration in Baoshan (31.3° N, 121.4° E) (Jiang, 1991), and are also in agreement with monthly evaporation in Xiamen (24.7° N, 118.5° E) (Fig. 2).

Then, we conducted precipitation case experiments based on above parameter values. As an example, only the sensitivity of the model to the B parameter is analyzed here.

2.2.2 Analysis of the experiment

Table 1 presents the values of parameters for 6 sub-experiments, i.e., Exps.a_1 and b_1 correspond to panel (a) in Fig. 3, Exps.c_1 and d_1 to (b), and Exps.e_1 and f_1 to (c). The experiment includes two cases, i.e., HTC and HMC, and the analysis is focused on r_{ai}, which is defined as the ratio of the surface runoff within a time step to the corresponding precipitation and is a measure for instantaneous runoff intensity.

In Fig. 3, the variations of r_{ai} for HTC are depicted with Curve A and Curve C, while those of r_{ai} for HMC are presented with Curve B and Curve D. The figure, shows that r_{ai} is very sensitive to the shape parameter B. For example, for HMC, corresponding to Fig. 3a, b and c ($W_0 = 90$ mm), B takes the values of 0.15, 0.3 and 0.5 respectively. The saturation starting time (r_{ai} reaches the maximum) is then 2.3, 3.7 and 5.3 days from Curve B, respectively; when simulation time $t = 1$ day, r_{ai} amounts to 21%, 32% and 42% respectively; when $t = 3$ days, r_{ai} reaches 77%, 66% and 58%, respectively. In Fig. 3a compared to Fig. 3b/c, because smaller values for B means less heterogeneity in infiltration capacity, different locations in the area reach the saturated state almost at the same time (i.e., r_{ai} reaches its maximum in a short time), and therefore the curve slope before the saturation starting time (i.e., when saturation is reached) is very steep (Curve B in Fig. 3a). Besides, a smaller value for B means

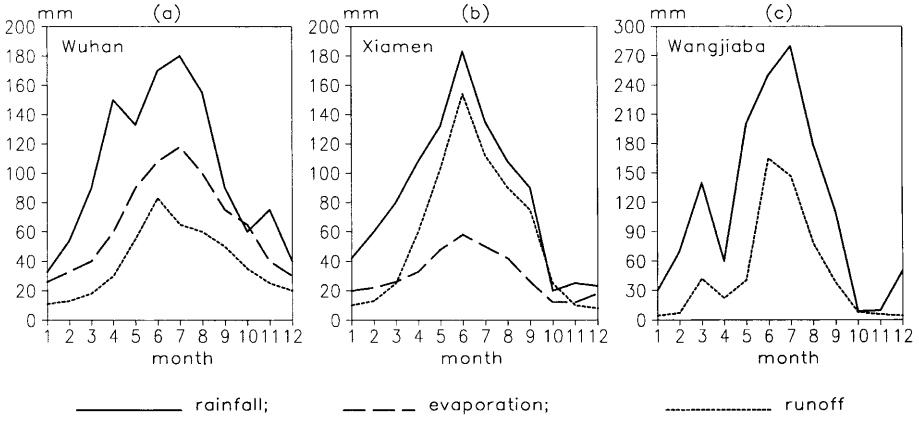

Fig. 2. Observations of surface moisture for three stations in the humid region of China, where (**a**) and (**b**) represent climatological surface moisture balance for Wuhan (30.6° N, 114.2° E) and Xiamen (24.7° N, 118.5° E), respectively, and (**c**) displays for the 1991 monthly precipitation and runoff for Wangjiaba (32.5° N, 115.4° E)

Table 1. Parameters in Exp.1 performed for B, where values for W_0 are initial ones

Test	B	B_e	k_b	μ	f_i	W_0 (mm)	W_c (mm)	E_{ps} (mm/s)	P_s (mm/s)
a_1	0.15	0.5	5×10^{-5}	0.6	0	90	130	6×10^{-5}	4×10^{-4}
b_1	0.15	0.5	5×10^{-5}	0.6	0	50	130	6×10^{-5}	4×10^{-4}
c_1	0.3	0.5	5×10^{-5}	0.6	0	90	130	6×10^{-5}	4×10^{-4}
d_1	0.3	0.5	5×10^{-5}	0.6	0	50	130	6×10^{-5}	4×10^{-4}
e_1	0.5	0.5	5×10^{-5}	0.6	0	90	130	6×10^{-5}	4×10^{-4}
f_1	0.5	0.5	5×10^{-5}	0.6	0	50	130	6×10^{-5}	4×10^{-4}

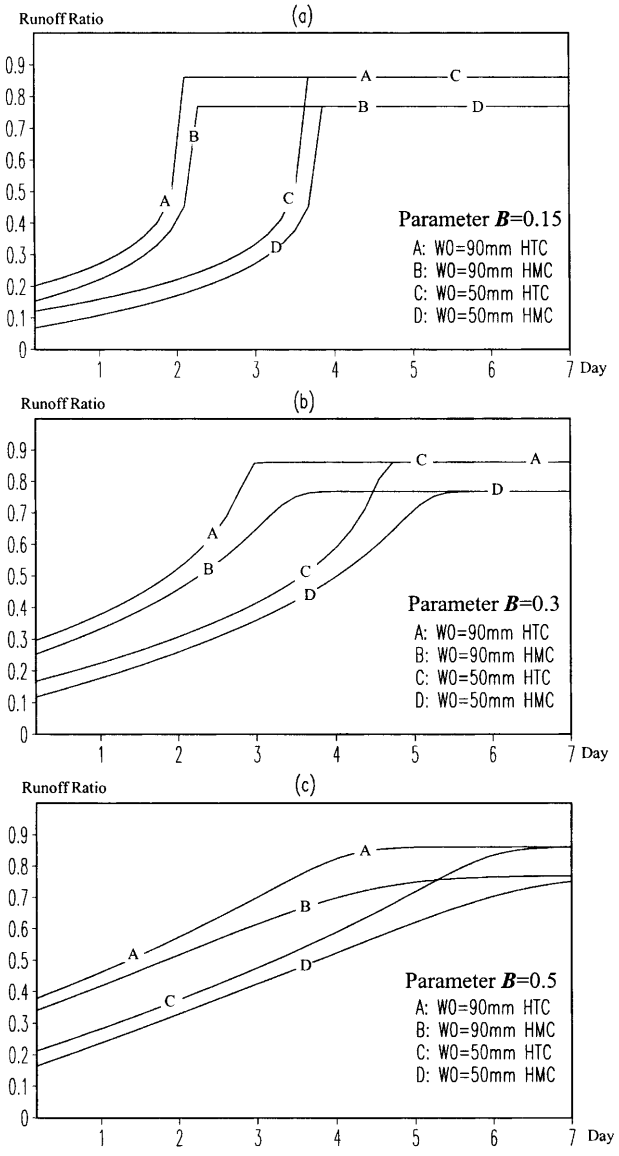

Fig. 3. Surface runoff ratio in Exp.1, where the variations of r_{ai} for HTC are depicted with Curves A and C, while those for HMC are presented with Curves B and D

greater infiltration capacity, therefore the value for r_{ai} is smaller for quite a long time before the saturation starting time (Curve B in Fig. 3a).

We are very interested in the effects of precipitation heterogeneity. In Fig. 3a, b and c, the maximum relative differences in r_{ai} between HMC and HTC can reach 43%, 20% and 12%, respectively, and the differences may be maintained for 0.2, 0.5 and 1.0 days. Additionally, the differences are larger than 5% all the time. These values imply large influences of precipitation heterogeneity on weather and therefore on climate.

Some regularities for different cases of B can still be identified in Fig. 3a, b and c, and this also confirms the large effects of precipitation heterogeneity. For example, at any moment, the value of Curve A (C) is greater than that of Curve B (D); the difference is at a maximum when the soil in the wetted area presented by Curve A/C becomes saturated, and it has an approximately constant value of about 10% after the soil presented by Curve B/D becomes saturated. This is because Curve A/C denotes HTC and the wetted fraction ($\mu = 0.6$) does not cover the whole area. Therefore if the soil moisture values are close for the two cases and the precipitation amounts are the same, the surface runoff for HTC (Curve A/C) is greater than that for HMC (Curve B/D). In addition, the moisture storage in the wetted fraction for HTC is greater than that for HMC, which implies that the runoff for HTC is greater than that for HMC afterwards. When the soils in both cases are saturated, with the soil for HMC demanding more and constant infiltration, the surface runoff for HTC is still greater than that for HMC and the difference remains stable. Considering that even if under the saturated condition there are still water losses due to evapotranspiration and base flow, which is of the order of 10% of precipitation, it is reasonable for $\sim$87% (Curve A/C) and $\sim$77% (Curve B/D) of precipitation to be transformed into surface runoff.

Curve A (B) is similar to Curve C (D) except that the former shows larger values of r_{ai} at the same time before saturation (while the values are close at saturation), and displays a longer period to reach the saturation due to initially drier soil conditions.

Other experiments (not shown because of space constraints) also demonstrate that the model is quite or even very sensitive to the parameters, i.e., B_e, k_b, μ, f_i, W_0 and W_c. These results show that appropriate values of the parameters can be chosen to reproduce realistic hydrological processes, based on which the model is incorporated into a regional climate model.

3. Application of VXM to regional climate modeling

3.1 Incorporation of VXM

In RegCM2, the surface runoff rate R_s is treated in two cases, i.e., when $T_{g1} < 273.16\,\mathrm{K}$ and $T_{g1} \geq 273.16\,\mathrm{K}$. In the first case, R_s is linear with respect to soil water; in the second,

$$R_s = \left(\frac{s_1 + s_2}{2}\right)^4 G, \tag{3}$$

where s_2 and s_1 are soil water relative to saturation at the surface layer and the root zone, respectively; G is the net water applied to the surface, which consists of three parts, i.e., rainfall P_r, snowmelt S_m, and evaporation F_q:

$$G = P_r + S_m - F_q. \tag{4}$$

Obviously, the treatment for surface runoff in RegCM2 is empirical and not physically based. In order to improve the description of hydrological processes at regional scales and to further improve the ability of regional climate modeling, here we modify VXM and then incorporate it into RegCM2, and hence obtain the augmented regional climate model ARCM. That is, we do not replace BATS in RegCM2 by VXM, and only apply the VXM calculation of surface runoff to BATS, while the VXM component for computing evapotranspiration is removed when VXM is incorporated. We use this method due to the following reasons: (1) The treatment of surface runoff is very important in hydrological models, and is the focus of model description. (2) Vegetation-atmosphere interactions are described in great detail in BATS, which can not be replaced by VXM. (3) Generally, land-surface schemes (e.g., BATS) account for the nonlinear interactions between surface temperature and moisture, while these interactions are usually not present in hydrological models (e.g., VXM). Hydrological models do not consider the effects of temperature unless temperature is involved in the calculation of evapotranspiration.

The only purpose of the incorporation of VXM is to substitute the calculation of surface runoff in BATS (therefore improve the regional climate modeling). Thus, after the input parameters (e.g., B, W_c, B_e, k_b, W_0, etc.) are added to BATS, the three terms in BATS, rainfall P_r, snowmelt S_m and evaporation F_q, should multiply the time step to replace P and E in VXM. In addition, if evaporation F_q is negative, let $E = 0$ with condensed water added into P.

In addition to taking the general values of parameters in sensitivity experiments of VXM, we follow BATS (Dickinson et al., 1993) and the nature of the infiltration capacity and soil moisture storage (Zhao, 1984), and prescribe the maximum soil moisture storage W_c, which is smaller in the south than in the north of China and generally varies between 120 mm and 160 mm, to be an empirical function of the subsurface layer temperature at a grid cell:

$$W_c = 4800 c_{wc}/(T_{g2} - 260), \tag{5}$$

where T_{g2} is the subsurface layer temperature, and generally, the constant c_{wc} equals 1.

And the initial value W_0 is here given as:

$$W_0 = c_{w0}[c_{ws}s_2 + (1 - c_{ws})s_1]W_c, \tag{6}$$

where c_{ws} is an input parameter ($c_{ws} = 0.5$ in the simulations), and generally, the constant c_{w0} equals 1. So, initially, W_0 is consistent with the climatic average of soil moisture in the BATS moisture initialization.

3.2 Experimental design

The model domain covers the area within 24.7–45.7° N and 100.88–133.12° E, which is centered at 35.20° N, 117.00° E. The grid resolution is 60 km with the grid number 41×40. Vertical levels of the model are set irregularly with 11 integral levels (i.e., $\sigma = 0.0$, 0.15, 0.30, 0.45, 0.60, 0.75, 0.85, 0.93, 0.97, 0.99, 1.00) and 10 half levels (for mostly output), which are located between 11 integral levels.

Table 2. Parameter values prescribed in ARCM

Test	B	k_b	μ	f_i	c_{w0}	c_{wc}	Test	B	k_b	μ	f_i	c_{w0}	c_{wc}
EXT01	–	–	–	–	–	–	EXT12	0.15	10^{-4}	–	0	1	1
EXT02	0.3	5×10^{-5}	–	0	1	1	EXT13	0.5	10^{-4}	–	0	1	1
EXT03	0.3	5×10^{-5}	0.4	0	1	1	EXT14	0.3	3×10^{-5}	–	0	1	1
EXT04	0.3	5×10^{-5}	0.6	0	1	1	EXT15	0.3	2×10^{-4}	–	0	1	1
EXT05	0.3	5×10^{-5}	0.8	0	1	1	EXT16	0.3	5×10^{-5}	0.6	0	0.65	1
EXT06	0.3	5×10^{-5}	1.0	0	1	1	EXT17	0.3	5×10^{-5}	0.6	0	1	1.5
EXT07	0.3	10^{-4}	–	0	1	1	EXT18	0.3	10^{-4}	0.6	0	0.65	1
EXT08	0.3	10^{-4}	0.4	0	1	1	EXT19	0.3	10^{-4}	0.6	0	1	1.5
EXT09	0.3	10^{-4}	0.6	0	1	1	EXT20	0.3	5×10^{-5}	0.6	0.15	1	1
EXT10	0.3	10^{-4}	0.8	0	1	1	EXT21	0.3	5×10^{-5}	0.6	0.3	1	1
EXT11	0.3	10^{-4}	1.0	0	1	1	EXT22	0.3	5×10^{-5}	0.6	0.075	1	1

The parameters prescribed for the coupled-model are given in Table 2. Note that the parameter μ represents the fraction of cumulus-convection precipitation, while we assume that large-scale precipitation covers the whole area of a grid cell (the amounts of the two kinds of precipitation can be derived from the outputs of BATS). Following the above initial conditions and the schemes for simulation in Table 2, we use the measured data for meteorological stations during the 1991 Meiyu season (i.e., May, June and July), and conduct experiments with ARCM apart from EXT01 that is performed with RegCM2. The experiments contain two groups, one is for HMC, which is symbolized with no value set for μ in Table 2, and the other is for HTC, to analyze the sensitivities and the mechanism in the experiments, after the consideration of PH and IH.

3.3 Analysis of experiments

3.3.1 Preliminary analysis of experiments for heterogeneities

The simulations for PH and IH are discussed at first using the 6 experiments, i.e., EXT01–EXT06 with $k_b = 5\times10^{-5}$, in which EXT01 employs RegCM2 and the others with μ increased gradually are conducted for PH and IH. Besides, EXT04 is taken as the control experiment.

Figure 4 compares the precipitation of EXT04 with the observations, which shows that the model can successfully reproduce the typical rainbelt in the Meiyu season over the Yangtze River-Huaihe River Valley in China. The investigated region (hereafter referred to as the JHR region) is located in the humid area, which contains the Xinanjiang Basin, the experimental site of the Xinanjiang model. Besides, due to the same lateral-boundary forcing, the model-produced circulation patterns and temperature fields can be comparable to observations (not shown).

Simulated results reveal that both the consideration of PH and IH can greatly influence land surface energy fluxes. From Table 3, it can be seen that the differences in the fluxes between EXT01 and EXT02, are several times larger than the differences between EXT02 and the experiment other than EXT01. For example, the differences in areally-averaged 3-month-mean sensible heat, latent heat and radiative fluxes for the JHR

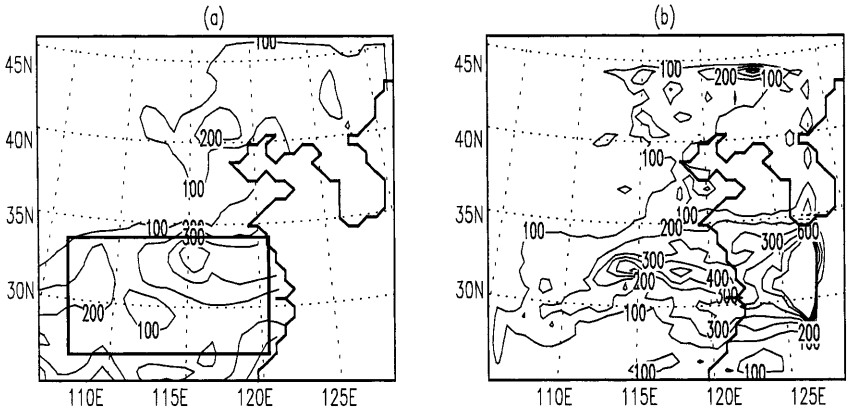

Fig. 4. Precipitation of observations and EXT04, where (**a**) displays observed monthly precipitation for June (mm) and the rectangle denotes the JHR region, and (**b**) is the same as (**a**) but for EXT04

Table 3. Simulated differences in areally-averaged 3-month-mean fluxes for JHR. (*SH*: sensible heat flux; *LH*: latent heat flux; *RF*: radiative flux; units: W/m^2)

Energy flux	Difference between EXT02 and EXT01	Difference between EXT02 and EXT03	Difference between EXT02 and EXT04	Difference between EXT02 and EXT05	Difference between EXT02 and EXT06
SH	8.5	3.8	− 2.5	4.4	− 2.0
LH	− 13.1	− 0.6	3.2	− 3.7	2.4
RF	4.4	0.7	1.2	− 1.1	2.3

region are $8.5\,W/m^2$, $-13.1\,W/m^2$ and $4.3\,W/m^2$, respectively. We suggest that these differences of surface fluxes are very large, as compared to the Earth's surface flux balance of CO2 doubling which would reduce the thermal radiation flux by about $4\,W/m^2$ (Houlton, 1997). Meanwhile, the differences in the fluxes between EXT02 and other experiments are still comparable to $4\,W/m^2$. It is these differences that lead to differences of distributions of surface air temperature, precipitation, etc.

The only difference between EXT01 and EXT02 lies in the consideration of IH in EXT02, while the differences between the experiments, EXT02–EXT06, are caused by the various extent of PH. Table 3 shows that the difference between EXT01 and EXT02 is the largest, therefore it may be concluded that effects of IH are greater than those of PH. This is because the differences in the average precipitation between different experiments are small under the given conditions (see analysis below), and that the changes of infiltration capacity characteristics may significantly modify the land surface climatology. Also, comparisons of other characteristics of EXT01–EXT06 exhibit the largest difference between EXT01 and EXT02 (not shown).

In addition, large differences between experiments with the same IH and different PH can still be identified. In Fig. 5a, during the first 5 days, the surface runoff ratio for JHR in EXT05 is larger than that in EXT02 by 6%; during the

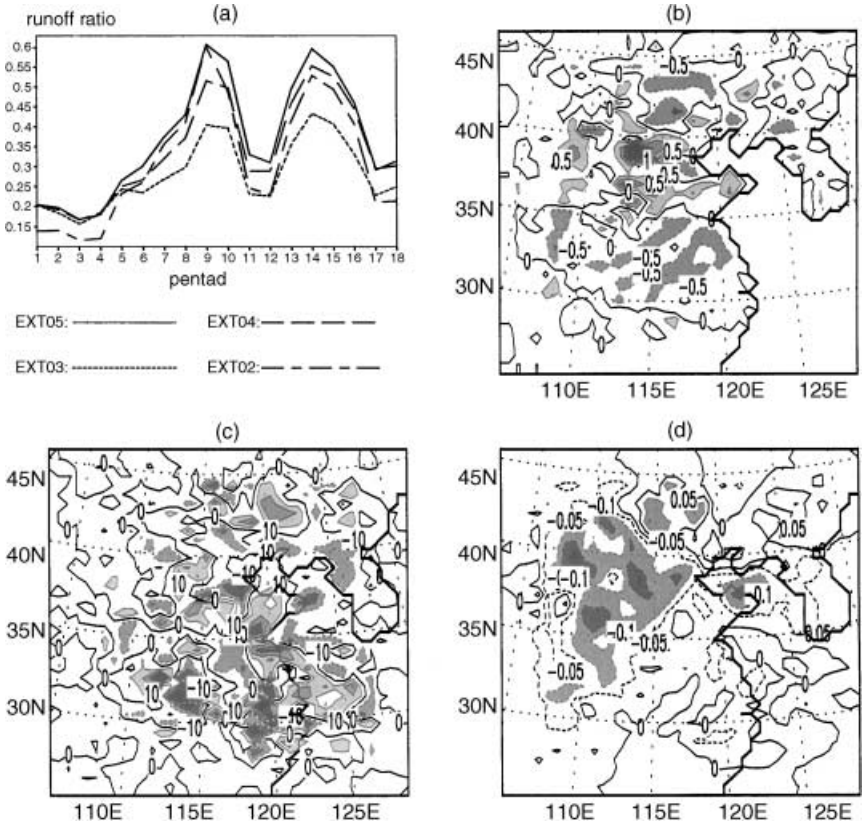

Fig. 5. Results from simulations for heterogeneities in precipitation and infiltration, where (**a**) displays 5-day-mean surface runoff ratios, (**b**) depicts the difference between the surface temperature in EXT02 and that in EXT03, contour interval is 0.5 K, and areas with absolute values of difference greater than 0.5 K are shaded, (**c**) presents the difference in 3-month-accumulated precipitation between EXT02 and EXT04, with contour interval of 10 mm and areas of absolute difference greater than 100 mm shaded, and (**d**) illustrates the 850 hPa-temperature difference between EXT02 and EXT04, with contour interval of 0.1 K, and areas of absolute difference greater than 0.1 K shaded

9th 5 day period, the surface runoff ratio in EXT05 (61%) is much larger than that in EXT02 (40%), and the surface runoff in EXT02 and EXT03 are respectively 39 mm and 23 mm, also a large difference. In fact, local differences can be much larger than the differences of average values due to the area (a grid cell) divided into rainfall and non-rainfall parts. So, owing to the differences of PH, hydrological processes may behave in very different ways.

Additionally, PH can affect the distributions of other quantities, such as soil moisture (not shown) and surface moisture balance (Fig. 6). As is shown in Fig. 5b, over large areas of the rainbelts of the northern China and the Yangtze River–Huaihe River Valley, the 3-month-mean surface temperatures in EXP03 are lower than those in EXP02 by more than 0.5 °C. We suppose that these differences of surface temperature are very large, in comparison with the increase of about 0.5 °C of the global warming during the last century or so (Houlton, 1997). Correspondingly at 850 hPa, the 3-month-mean temperatures in EXP03 are lower than those in EXP02 by more than 0.1°C (not shown). Figure 5c–d depict the differences between EXT02 and EXT04 due to including PH, in which a systematic bias of 850 hPa-air-temperature due to different extents of PH can be identified. It should be noted that this bias is generally lower than the bias between simulations and observations (not shown), i.e., no significant improvement in temperature is achieved.

From the simulations of EXT01 and EXT02, we can identify the large effects due only to IH. Over the vast area of the Yangtze River-Huaihe River Valley, the 3-month-mean 850 hPa temperatures in EXP01 are lower than those in EXP01 by more than 0.2 °C; and the mean surface temperatures in EXP01 are lower by 0.5–1.5 °C (not shown). Therefore, the surface and lower-layer temperatures simulated with ARCM are generally higher than those with RegCM2. The reason for the temperature change is, that the decrease of infiltration (i.e., the increase of

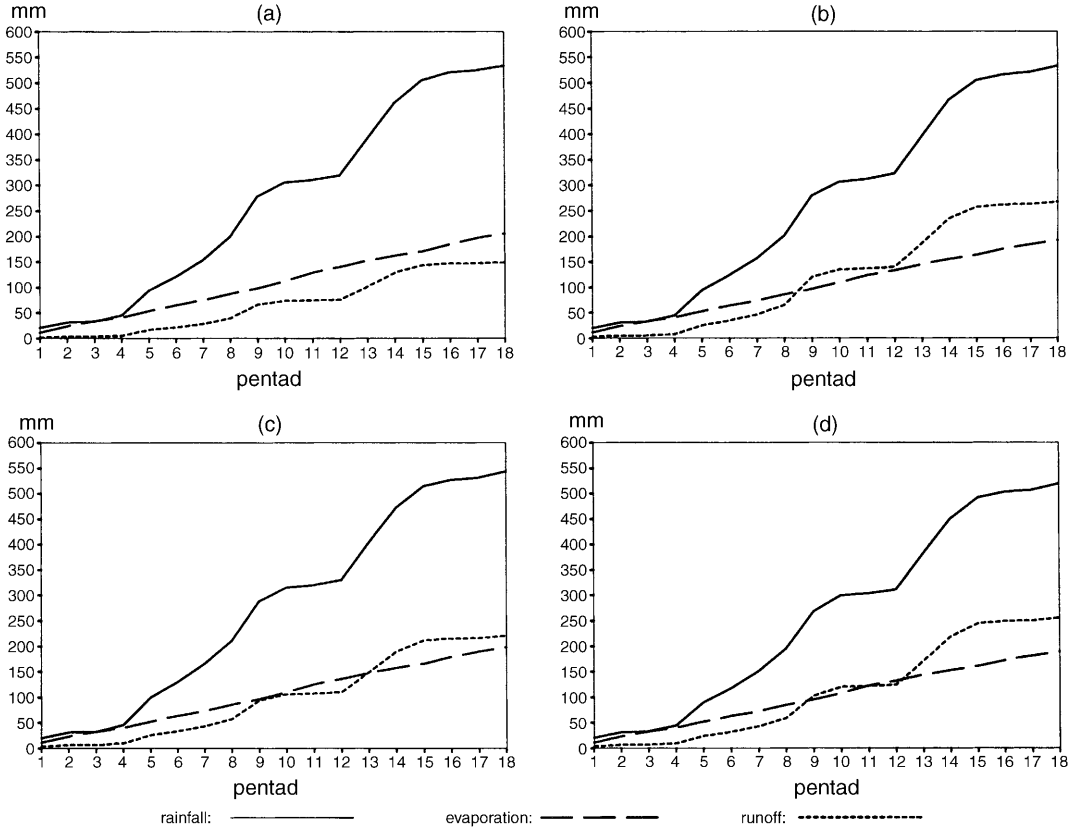

Fig. 6. Accumulated rainfall, evapotranspiration and runoff in units of mm once every 5 days: (**a**) EXT01, (**b**) EXT02, (**c**) EXT03, and (**d**) EXT04

Table 4. Simulated characteristic quantities for the JHR region (around Yangtze River-Huaihe River Valley), in which P_m, R_m, P_a, and r_a respectively represent the maximum 3-month accumulated precipitation, maximum 3-month accumulated surface runoff, areally-averaged 3-month-mean precipitation and areally-averaged 3-month-mean surface runoff ratio; and P_j is the maximum precipitation for June

Test	P_m (mm)	R_m (mm)	P_a (mm)	r_a (%)	P_j (mm)	Test	P_m (mm)	R_m (mm)	P_a (mm)	r_a (%)	P_j (mm)
EXT01	1439	691	538	28.0	615	EXT12	1575	1232	548	44.4	569
EXT02	1523	1188	540	50.2	597	EXT13	1637	1298	532	46.8	761
EXT03	1625	1158	550	40.6	725	EXT14	1556	1302	540	53.4	605
EXT04	1566	1243	524	49.2	638	EXT15	1572	1154	540	39.2	735
EXT05	1352	1067	532	51.8	627	EXT16	1710	1349	545	44.9	667
EXT06	1683	1419	545	51.6	631	EXT17	1692	1058	543	37.3	660
EXT07	1544	1210	534	45.0	897	EXT18	1412	1007	539	41.7	693
EXT08	1717	1227	541	36.6	672	EXT19	1547	1067	546	34.8	600
EXT09	1383	1017	545	45.4	591	EXT20	1594	1327	524	55.4	631
EXT10	1481	1101	548	48.3	680	EXT21	1584	1370	518	60.5	569
EXT11	1375	1044	538	46.6	578	EXT22	1554	1236	535	51.3	895

surface runoff) leads to a decrease of soil moisture and therefore a decrease of evapotranspiration (resulting in less cooling of the surface) and soil heat storage, and further leads to the higher temperatures, after IH is taken into account. The relation between soil moisture and surface temperature is in agreement with the results of data analysis in Walsh et al. (1985) and with those of numerical simulations (e.g., Stamm and Wood, 1994).

As for precipitation amounts, there may be quite large differences in the precipitation distributions among the experiments, however, the differences in the regional averages over the JHR region are very small. For instance, in Table 4, the maximum 3-month accumulated precipitation amounts (P_m) in EXT05 and EXT06 are 1352 mm and 1683 mm, and the regional averages of precipitation amount (P_a), are 532 mm and 545 mm, respectively. In addition, at small time scales (e.g., several days), precipitation amounts have considerable spatial and temporal variability. Obviously, the accumulation of these large variations do not produce large differences in P_a. The reason is that the solution in the interior of a regional model domain is essentially determined by the dynamical equilibrium of lateral boundary information and internal model physics (Giorgi and Mearns, 1999), in which the land surface heterogeneity plays a less important role. Owing to the effects of heterogeneities at small time scales (e.g., several days), the variation of precipitation can be quite large, however, due to the same lateral boundary forcing, at larger time scales (e.g., monthly or seasonal scale), the variation of precipitation may be relatively small.

Table 4 lists the results of the surface runoff for the JHR region, e.g., the values of the mean surface runoff ratio, r_a, in EXT01, EXT02, EXT03, EXT04, EXT05 and EXT06 are 28.0%, 50.2%, 40.6%, 49.2%, 51.8% and 51.6%, respectively, which is consistent with what is illustrated in Fig. 6. The result (i.e., the surface runoff is increased after IH is included) is very consistent with the observed climatology. Some annual components of the surface moisture over the humid region of China are shown in Fig. 2: the surface runoff ratio in Wuhan (30.6° N, 114.2° E) exceeds 40%, as also does the runoff ratio in Wangjiaba (32.5° N, 115.4° E) for the 3 months, May–July, in 1991 as a whole, which is very close to the values of runoff ratio simulated with the inclusion of IH. Besides, for June and July, the monthly mean surface runoff exceeds the monthly mean evaporation over the JHR region (Fig. 6b, c, d), which agrees with the general case for very humid areas (e.g., Xiamen and Wangjiaba in Fig. 2), and which is consistent with the fact that an extremely heavy flood occurred in the JHR region in 1991. This confirms the conclusion that improving the realism of the areal distribution of precipitation can alter the balance between runoff and evaporation (Pitman et al., 1990). Compared to RegCM2, ARCM enhances the runoff ratio from 28% to

more than 40%. Liu et al. (1994) simulated the regional climate of East Asia for June–August 1990 with RegCM2, as for the summer average water fluxes. The ratio of evapotranspiration to precipitation was very close to 80%, and the ratio of runoff to precipitation close to 20% over the humid region of Central China (shown in their Fig. 16 for Region 2 that includes the JHR region used here). The result is in agreement with that for EXT01, considering 1990 to be a normal year. Thus, in general, RegCM2 has a bias that underestimates runoff over humid regions in China, while the simulations with ARCM is consistent with a realistic climatology.

Note that there is an obvious improvement due to IH concerning runoff ratio (even the ratio of 40.5% in EXT03 is quite large as compared to 28.0% in EXT01), no large runoff-ratio difference can be seen between EXT02 and EXT03–EXT06. This also confirms that the effects due to including IH are larger than those due to including PH.

Similarly, when the simulations (EXT07–EXT11) in the case of $k_b = 10^{-4}$ are examined (see Table 4), the same conclusions can be drawn.

3.3.2 Sensitivity study of ARCM to VXM parameters

(a) Parameter B. In EXT12, EXT07 and EXT13, model conditions are the same except for different values of B, i.e., 0.15, 0.3 and 0.5 for EXT12, EXT07 and EXT13, respectively. With the same maximum soil moisture storage W_c, different values of B reflect different features of IH. It can be drawn from Fig. 7, that ARCM is quite sensitive to the value of B (i.e., to the infiltration feature). For instance, the positive-value center of precipitation difference between EXT12 and EXT07 is larger than 500 mm. The area with precipitation difference greater than 100 mm is also quite large (Fig. 7a); shown in Fig. 7b, there apparently is a systematic temperature increase at 850 hPa in EXT13 compared to EXT12 (owing to the greater B in EXT13), and the area with temperature change over 0.1 °C is substantial. Curve A shown in Fig. 3a, b and c, with the same W_c, greater B causes less infiltration initially, less humid soil and therefore a longer time to reach saturation; though the runoff ratios are the same at saturation due to the same W_c, the duration of greater runoff ratio is longer for the case of greater B. Generally the soil is unsaturated, hence greater B means less infiltration and less humid soil, which leads to higher temperatures in the low-level atmosphere. Correspondingly, there is also an apparent systematic temperature increase at the land surface (with the maximum 2.3 °C) in EXT13 compared to EXT12 (not shown). Due to the same lateral boundary forcing, all obvious differences lie in the interior of the domain.

(b) Parameters W_0 and W_c. In order to investigate the sensitivity of ARCM results to the two parameters, i.e., initial soil moisture storage W_0 and the maximum soil moisture storage W_c, we design the experiment EXT16, in which the value of W_0 is 65% of that in EXT04 (the control experiment), and the experiment EXT17, in which the value of W_c is 1.5 times as much as that in EXT04. So, the ratio of W_0 to W_c in EXT16 (EXT17) is 0.65 (0.67) times as much as that in EXT04.

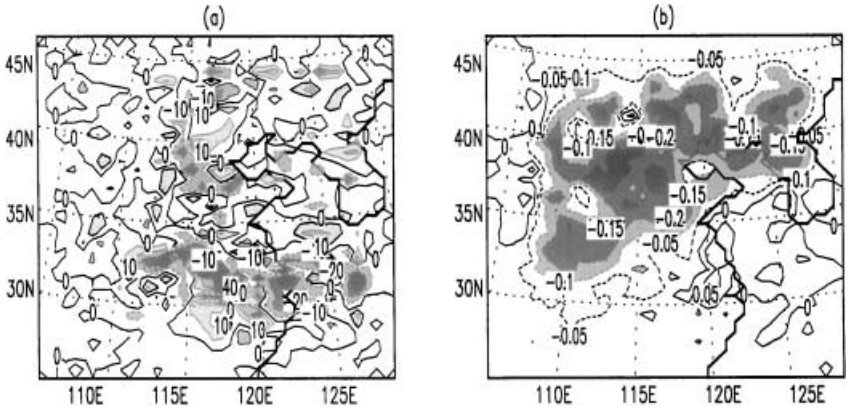

Fig. 7. Comparison of ARCM results dependent on B: (**a**) same as Fig. 5c but for the difference between EXT12 and EXT07, (**b**) same as Fig. 5d but for the difference between EXT12 and EXT13

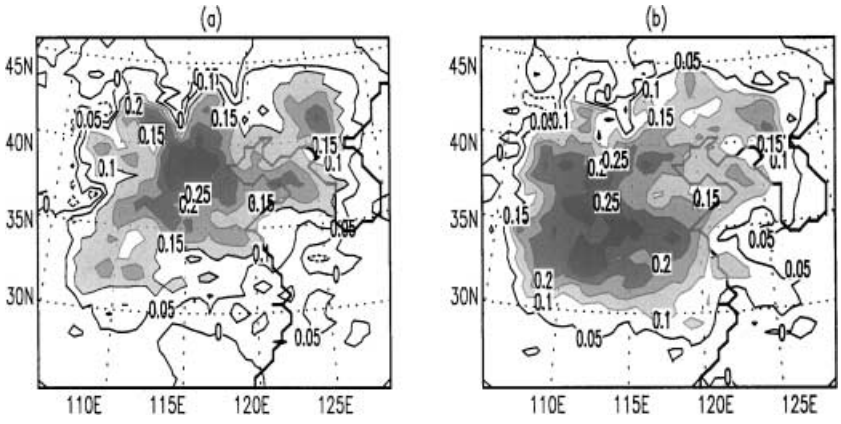

Fig. 8. Comparison of ARCM results dependent on W_0 and W_c, where (**a**) illustrates the difference in 850 hPa temperature between EXT04 and EXT16, with contour interval of 0.1 K, and areas of absolute values of difference greater than 0.1 K shaded, and (**b**) is the same as (**a**) but for the difference between EXT04 and EXT17

Figure 8a depicts the 850 hPa-temperature differences between EXT04 and EXT16, in which the differences are generally greater than 0 °C and can amount to 0.30 °C; Fig. 8b displays the differences between 850 hPa temperatures in EXT04 and those in EXT17, in which the differences are even greater than those in Fig. 8a, as is the change in the surface temperature. For example, for the average temperature over the JHR region, the value in EXT04 is 0.31 °C higher than that in EXT16 and 0.42 °C higher than that in EXT17, respectively. Due to the small initial moisture storages, the soil in EXT16 and EXT17 needs more water to generate runoff; therefore the water increases the soil moisture and leads to lower surface temperature. So, ARCM is very sensitive to the initial soil moisture storage and the maximum infiltration capacity. Note that the surface temperature in EXT16 is higher than that in EXT17. Therefore ARCM is less sensitive to the initial soil moisture storage than to the maximum infiltration capacity, which reflects land surface features such as soil texture and topography. In other words, at seasonal scale the surface features are more important than the initial soil water.

The above conclusion for the sensitivity to W_0 and W_c is further demonstrated in Table 4, which shows that the runoff ratios of EXT04, EXT16 and EXT17 are 49.2%, 44.9% and 37.7%, respectively. This also confirms the appropriatness of the consideration for W_0 and W_c in the control experiment (EXT04).

(c) Parameter f_i. The designer of the Xinanjiang model considered the impermeable fraction f_i in the model. The parameter is necessary for semi-arid regions due to hardened and impervious soil. So taking this parameter into account we might find some effects of land-use change (e.g., aridification). The model conditions in the experiments, EXT04, EXT20 and EXT21, are the same except for the different values of f_i (0, 0.15 and 0.3 for EXT04, EXT20 and EXT21, respectively).

Figure 9a illustrates the differences in the accumulated runoff between EXT04 and EXT21, and shows that the accumulated runoff in EXT21 is generally much greater than those in EXT04 except that those in the JHR region in EXT04 are slightly larger due to different distribution of precipitation. This indicates that the consideration of the impermeable fraction in the model can greatly modify the surface hydrology.

Figure 9b displays the differences in the surface temperature. For the JHR region, the surface temperatures in EXT04 are generally lower than those in EXT21 by an average of 0.74 °C (with a maximum of 2.6 °C); correspondingly at 850 hPa for the region (not shown), the temperatures in EXT04 are generally lower than those in EXT21 by an average of 0.31 °C (with a maximum of 0.57 °C). The comparison of EXT04 and EXT20 is similar. Therefore, the surface temperature (or the low-level air temperature) arises with the increase of the impermeable fraction. The reason is, that under the condition of small

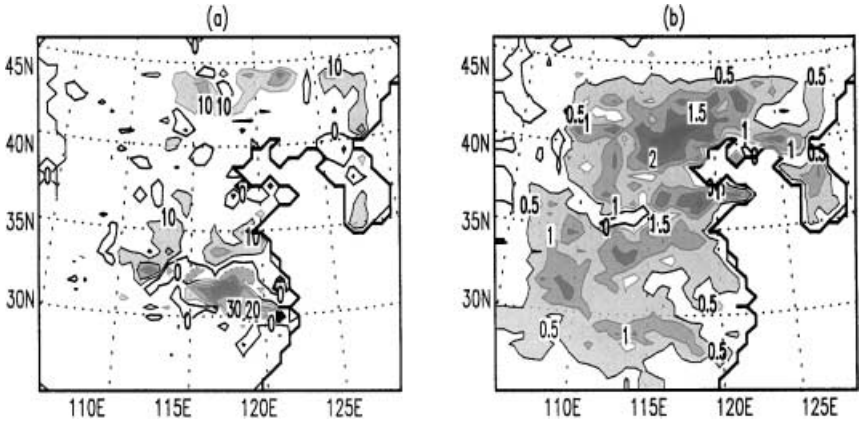

Fig. 9. Comparison of ARCM results dependent on f_i, where (**a**) is the same as Fig. 5c but for the accumulated-runoff difference between EXT04 and EXT21, (**b**) the same as Fig. 5b but for the difference between EXT04 and EXT21

changes of average precipitation (as is analyzed above), with the decrease of infiltration, i.e., with a larger value of f_i, the soil moisture decreases and therefore the temperatures increase. All together this shows that the effect of aridification on temperatures is substantial.

4. Summary and discussion

In this paper, firstly, an off-line hydrological model (VXM) was developed to account for subgrid heterogeneities in soil infiltration capacity and precipitation. VXM is a combination of the Xinanjiang model and the VIC model, and is mainly characterized by its runoff-generating parameterization suitable for application over humid areas. Then, off-line VXM experiments were performed to test its sensitivity to the parameters, and some conclusions consistent with observation were obtained. This confirmed, the feasibility of the incorporation of VXM into the regional climate model RegCM2.

The main purpose of this study is to investigate the effects of subgrid precipitation and infiltration heterogeneities and to further improve regional climate modeling. We incorporated VXM into RegCM2 (this climate model is referred to as ARCM). This approach is different from some previous regional-climate studies (e.g., Giorgi et al., 1993a,b; Giorgi and Mearns, 1999) for it is allowing detailed atmosphere-biosphere-hydrology interactions. Applying station data during the 1991 Meiyu season (May, June and July) as the initial and boundary conditions of ARCM, sensitivity experiments were conducted.

We found that the regional climate and surface hydrology are quite sensitive to the two heterogeneities, i.e., the simulations for the surface fluxes, soil temperature and moisture, precipitation and surface runoff can be considerably affected by the heterogeneities. The consideration of infiltration heterogeneity in ARCM can effectively improve the simulation of hydrological processes, i.e., it can greatly enhance the runoff ratio, which is consistent with observations over the humid region of China. This implies that it is necessary to consider the heterogeneity within the region, and through feedbacks, effects, the climate modeling may be improved in some sense.

It seems that the influence of infiltration heterogeneity on the regional surface climate is greater than that of precipitation heterogeneity. This is because the model's climate is essentially determined by lateral boundary information and internal model physics, in which the atmospheric processes, e.g., atmospheric dynamics and physics (the same in both models), may play a more important role for precipitation than land surface processes, while land surface features, e.g., the surface infiltration heterogeneity, may exert more direct and stronger effects on surface climate.

It is also shown that the modeled climate is sensitive to the parameters of the VXM model. For instance, larger B may cause a warmer and less humid surface; the model's climatology is greatly modified after the impermeable fraction at the surface has been taken into account, which may imply some aridification effects and that the fraction should be increased in long-term climate simulations due to the aridification trend.

In general, the capability of regional climate models to simulate the surface climate can be improved by appropriate subgrid-heterogeneity representation. In addition, the sensitivity tests imply that for each sub-region, model parameters

should be calibrated using real data (e.g., daily river runoff data). Therefore, further validation of the model for applications is a task that remains for a follow-up study.

It should be noted, that due to the limitation of our computational resources, the domain area is not very large. However, it is adequate for the sensitivity investigation and generally will not affect the main conclusions drawn above. In fact, the sensitivities analyzed above are not overestimated compared to those obtained from models with a larger model domain. Generally, the farther from the lateral boundaries, the stronger the heterogeneity effect becomes, due to the same lateral boundary forcings. Therefore, more heterogeneity-induced information of mesoscale climatology is contained in a larger domain in the regional models. Hence, the model domain should be enlarged for more practical studies in the future.

Appendix

1. Treatments for homogeneous precipitation

At a grid cell, infiltration heterogeneity (IH) can be represented by (Wood et al., 1992)

$$i = i_m[1 - (1 - A)^{1/B}], \tag{A1}$$

where i and i_m are the infiltration capacity and the maximum infiltration capacity, respectively, A is the fraction of an area for which the infiltration capacity is less than i, and B denotes the infiltration shape parameter. Thus, if initially $i = i_0$, and after a time step the area receives a precipitation amount P, the surface runoff Q_d can be computed by

$$Q_d = \int_{i_0}^{i_0+P} A(i)di. \tag{A2}$$

In fact, Q_d is the portion of P which precipitates over the saturated fraction A_s, and therefore the infiltration is $P - Q_d$. Then W_c and W_0 can be derived from

$$W_c = \frac{i_m}{1+B}, \tag{A3}$$

$$W_0 = W_c\left[1 - \left(\frac{i_m - i_0}{i_m}\right)^{B+1}\right]. \tag{A4}$$

Hence, given the parameters B, W_c, i_0 and P, the surface runoff within the time step Q_d can be written as

$$Q_d = P - W_c + W_0 \quad \text{for } i_0 + P \geq i_m, \tag{A5}$$

and

$$Q_d = P - W_c + W_0 + W_c\left[1 - \frac{i_0 + P}{i_m}\right]^{1+B} \quad \text{for } i_0 + P < i_m. \tag{A6}$$

Evapotranspiration E and base flow Q_b in VXM are the same as Wood et al. (1992):

$$E = E_p\left[1 - \left(1 - \frac{W_0}{W_c}\right)^{1/B_e}\right], \tag{A7}$$

and

$$Q_b = k_b W_0, \tag{A8}$$

where the parameter k_b varies within [0, 1].

2. Treatments for heterogeneous precipitation

In VXM, the heterogeneous-precipitation case is similar to the homogeneous-precipitation case. Following Liang et al. (1996), we also assume that the point convective precipitation intensity is exponentially distributed over the fraction μ of the grid area. Since the RCM time step is small, it is convenient to assume that the precipitation amount within a time step is exponentially distributed as

$$f(P_k) = \frac{\mu}{P}\exp\left(-\frac{\mu P_k}{P}\right), \tag{A9}$$

where $f(P_k)$ is the probability of precipitation that is larger than P_k. Assume x to be the percentage that receives a precipitation amount greater than or equal to P_k over the fraction μ, then

$$x = 1 - \int_0^{P_k} f(P_k)dP_k = \exp\left(-\frac{\mu P_k}{P}\right), \quad 0 < x \leq 1. \tag{A10}$$

Similar to the HMC, Q_d includes two terms, i.e.,

$$dQ_d = [P_k(x) - W_c + W_0]dx \qquad \text{for } i_0 + P \geq i_m \tag{A11a}$$

and

$$dQ_d = \left\{P_k(x) - W_c + W_0 + W_c\left[1 - \frac{i_0 + P}{i_m}\right]^{1+B}\right\}dx \quad \text{for } i_0 + P < i_m. \tag{A11b}$$

If a satisfies $i_0 + P_k(a) = i_m$, Q_d can be derived from combining the above two terms:

$$Q_d = P - \mu(W_c - W_0) + \mu W_c\int_a^1\left[1 - \frac{i_0 - \frac{P}{\mu}\ln x}{i_m}\right]^{1+B}dx. \tag{A12}$$

For details, see Liang et al. (1996). Besides, computing other quantities in HTC is similar to that in HMC.

Acknowledgements

This work is supported by the Chinese NKBRSF Project G1999043400 and MEC Grant No. 20010284027. The authors would like to thank two anonymous reviewers for their comments on this work.

References

Avissar R, Pielke RA (1989) A parameterization of heterogeneous land surface for atmospheric numerical models and its impacts on regional meteorology. Mon Wea Rev 117: 2113–2136

Beven KJ, Kirkby MJ (1979) A physically based variable contributing area model of basin hydrology. Hydrol Sci Bull 24: 43–69

Dickinson RE, Henderson-Sellers A, Kennedy PJ, Wilson MF (1993) Biosphere/Atmosphere Transfer Scheme (BATS) Version le as Coupled to the NCAR Community Climate Model. NCAR Tech Note TN-387 + STR, National Center for Atmospheric Research, Boulder, CO

Eagleson PS (1984) The distribution of catchment coverage by stationary rainstorms. Water Resour Res 20: 581–590

Eagleson PS, Wang Q (1985) Moments of catchment storm area. Water Resour Res 21: 1185–1194

Eagleson PS, Fennessey NM, Wang Q, Rodriguez-Iturbe I (1987) Application of Poisson models to air mass thunderstorm rainfall. J Geophys Res 92: 9661–9678

Entekhabi D, Eagleson P (1989) Land surface hydrology parameterization for the atmospheric general models including subgrid-scale spatial variability. J Climate 2: 816–831

Famiglietti JS, Wood EF (1994) Multiscale modeling of spatially variable water and energy balance processes. Water Resour Res 30: 3061–3078

Francini M, Pacciani M (1991) Comparative analysis of several conceptual rainfall-runoff models. J Hydrol 122: 161–219

Gao X, Sorooshian S (1994) A stochastic precipitation disaggregation scheme for GCM applications. J Climate 7: 238–247

Giorgi F, Avissar R (1997) Representation of heterogeneity effects in earth system modeling: Experience from land surface modeling. Rev Geophys 34: 413–437

Giorgi F, Marinucci MR, Bates GT (1993a) Development of a second generation regional climate model (REGCM2), Boundary layer and radiative transfer processes. Mon Wea Rev 121: 2794–2813

Giorgi F, Marinucci MR, DeCanio G, Bates GT (1993b) Development of a second generation regional climate model (REGCM2), Cumulus cloud and assimilation of lateral boundary conditions. Mon Wea Rev 121: 2814–2832

Giorgi F, Mearns LO (1999) Introduction to special section: Regional climate modeling revisited. J Geophys Res 104: 6335–6352

Horton RE (1933) The role of infiltration in the hydrological cycle. Eos Trans AGU 14: 446–460

Houlton J (1997) Global warming: the complete briefing. United Kingdom: Cambridge University Press pp 18–20

Jiang D (1991) The climate of the upper and lower reaches of Yangtze River. China: The Meteorology Press pp 1–246 (in Chinese)

Koster R, Suarez M (1992) Modeling the landsurface boundary in climate models as a composite of independent vegetation stands. J Geophys Res 97: 2697–1715

Liang X, Lettenmaier DP, Wood EF, Burges SJ (1994) A simple hydrologically based model of land-surface water and energy fluxes for general circulation models. J Geophys Res 99: 14415–14428

Liang X, Lettenmaier DP, Wood EF (1996) One-dimensional statistical dynamic representation of subgrid spatial variability of precipitation in the two-layer variable infiltration capacity model. J Geophys Res 101: 21403–21422

Liu Y, Giorgi F, Washington WM (1994) Simulation of summer monsoon climate over east Asia with an NCAR regional climate model. Mon Wea Rev 122: 2231–2348

Peters-Lidard CD, Zion MS, Wood EF (1997) A soil-vegetation-atmosphere transfer scheme for modeling spatially variable water and energy balance processes. J Geophys Res 102: 4303–4324

Philip JR (1957) The theory of infiltration, 1. The infiltration equation and its solution. Soil Sci 83: 345–357

Pitman AJ, Henderson-Sellers A, Yang ZL (1990) Sensitivity of regional climates to localized precipitation in global models. Nature 346: 734–737

Sellers P, Randll DA, Collatz GJ et al. (1996) A revised land surface parameterization (SiB2) for atmospheric GCMs, Part I: model formulation. J Climate 9: 675–705

Sheng C (1986) Survey of China Climate. The Science Press, China, 1–354 (in Chinese)

Sivapalan M, Beven K, Wood EF (1987) On hydrologic similarity: 2. A scaled model of storm runoff production. Water Resour Res 23: 2266–2278

Sivapalan M, Woods RA, Kalma JD (1997) Variable bucket representation of TOPMODEL and investigation of the effects of rainfall heterogeneity. Hydro Proces 11: 1307–1330

Smith RE, Hebbert RHP (1983) Mathematical simulation of interdependent surface and subsurface hydrologic processes. Water Resour Res 19: 987–1001

Stamm JF, Wood EF (1994) Sensitivity of a GCM simulation of global climate to the representation of land-surface hydrology. J Climate 7: 1218–1239

Walko RL, Band LE, Baron J et al. (2000) Coupled atmosphere-biophysics-hydrology models for environmental modeling. J Appl Meteor 39: 931–944

Walsh JE et al. (1985) Land-surface fluctuation and associated climatic variability. Third conference on climate variations and symposium on contemporary climate, 1850–2100, 85–86, Los Angels

Wood EF, Lettenmaier DP, Zartarian VG (1992) A land-surface hydrology parameterization with subgrid variability for general circulation models. J Geophys Res 97: 2717–2728

Warrilow DA, Sangster AB, Slingo A (1986) Modeling land surface processes and their influence on European climate. Dyn Clim Tech Note 38: 92 pp, U.K. Meteorol Off, Bracknell, Berkshire, England

Yu Z (2000) Assessing the response of subgrid hydrologic processes to atmospheric forcing with a hydrologic model system. Glob Plan Change 25: 1–17

Zhao R (1984) Basin Hydrologic Models – the Shanxi Model and the Xinanjiang Model. China: The Electric-Power and Water-Conservancy Press, pp 1–180 (in Chinese)

Authors' addresses: Dr. Zeng Xinmin, Department of Atmospheric Sciences, Nanjing University, Nanjing 210093, People's Republic of China; J. Chen, Department of Earth Science, Nanjing University, Nanjing 210093, People's Republic of China; M. Zhao, B.-K. Su, J.-P. Tang, Y.-Q. Zheng, Key Laboratory for Mesoscale Severe Weather of Ministry of Education, Nanjing University, Nanjing, P.R. China; Y.-J. Zhang, Cold and Arid Regions Environmental and Engineering Research Institute, Lanzhou, P.R. China.